공학석사 학위논문

Label Compound Trapped Ag Nano-gap Bumpy Shell for Highly Sensitive Surface-Enhanced Raman Scattering

표지자가 끼어있는 은 나노갭 범피쉘의 합성과 표면증강 라만산란으로의 응용

2015년 2월

서울대학교 대학원

화학생물공학부

이 현 미

Label Compound Trapped

Ag Nano-gap Bumpy Shell for Highly Sensitive

Surface-Enhanced Raman Scattering

표지자가 끼어있는 은 나노갭 범피쉘의 합성과

표면증강 라만산란으로의 응용

지도 교수 이 윤 식

이 논문을 공학석사학위논문으로 제출함

2015년 2월

서울대학교 대학원

화학생물공학부

이 현 미

이현미의 공학석사학위논문을 인준함

2014년 12월

위 원 장 장 정 식 (인)

부위원장 이 윤 식 (인)

위 원 이 종 협 (인)

Abstract

Label Compound Trapped Ag Nano-gap Bumpy Shell for Highly Sensitive Surface-Enhanced Raman Scattering

라만 표지자가 끼어있는 은 나노갭 범피쉘의 합성과 표면증강 라만산란으로의 응용

Hyunmi Lee

School of Chemical & Biological Engineering

The Graduate School

Seoul National University

Surface-enhanced Raman scattering (SERS) is an ultrasensitive vibrational spectroscopic technique which has been applied to various analytical area, especially in bio-sensing and bio-imaging. Recently, this

technique has been used to design novel SERS tags consisting of noble metallic nanoparticles (NPs) and specific Raman reporter molecules (RMs). However, the conventional synthetic approaches for SERS tags have been suffered from multi-step and low signal stability. Previously, single-step synthesis of Ag nanoshells (Ag NSs) were reported by our group. In the present work, a further study was performed on the single-step synthesis of SERS tags having nano-gap structure leading to generate highly enhanced unique Raman signal. Ag nano-gap bumpy shells (Ag NBSs) were successfully synthesized in single-step. This unusual burst growth of Ag NBSs was attributed to simultaneous addition of small RMs to reaction media, which in turn led to small Ag NPs formation and simultaneous adsorption of both Ag NPs and RMs. Ag NBSs showed substantially enhanced Raman intensity and better stability over one month period of storage than Ag NSs-based SERS tags prepared by conventional method. Furthermore, various kinds of Ag NBSs were prepared using different Raman RMs, and the possibility for use as multiplex cellular imaging was demonstrated.

Keyword : Surface-enhanced Raman scattering, nanoshell, nano-gap, multiplex detection.

Student Number : 2013-20987

TABLE OF CONTENTS

LIST OF FIGURES

NBSs).

Figure 3.5 Comparison of intensity and stability between Ag NSs and Ag NBSs with the 785 nm photo-excitation of 30 mW laser power and light acquisition time of 1 s.

Figure 3.6 Multiplexing capability of Ag NBSs. SERS spectra of Ag NBS trapped simple aromatic compounds such as 2-CBT, 4-CBT, 4-BBT, 2-FBT and 4-FBT were obtained with the 785 nm photo-excitation of 30 mW laser power and light acquisition time of 1 s.

Figure 3.7 (a)-(d) Bright field images for two different types of lung cancer cell lines, A549 and H522. A549 cell lines were treated (a),(e),(i),(m) EGFR-Ag $NBSs_{[4\text{-}FBT]}$ and (c),(g),(k),(o) HER2-Ag $NBSs_{[2\text{-}FBT]}$. H522 cell lines were treated (b),(f),(j),(n) EGFR-Ag $NBSs_{[4\text{-}FBT]}$ and (d),(h),(l),(p) HER2-Ag $NBSs_{[2\text{-}FBT]}$. SERS mapping of corresponding cell lines were measured at (e),(f) 623 cm^{-1} (4-FBT) displayed in green and at (g),(h) 494 cm^{-1} (2-FBT) displayed in purple. (i)-(l) Merged SERS mapping images, (m)-(p) SERS spectra of A549 and H522 cell lines using the 785 nm photo-excitation of 7.5 mW laser power and light acquisition time of 1 s.

Figure 3.8 H522 cell lines were treated with a mixture (EGFR-Ag $NBSs_{[4\text{-}FBT]}$ and HER2-Ag $NBSs_{[2\text{-}FBT]}$). (a) Bright field images for H522

cell lines. SERS mapping of corresponding cell lines were measured at (b) 494 cm^{-1} (2-FBT) displayed in purple and at (c) 623 cm^{-1} (4-FBT) displayed in green. (d) Merged SERS mapping, (e) SERS spectra of H522 cell lines were obtained using the 785 nm photo-excitation of 7.5 mW laser power and light acquisition time of 1 s.

LIST OF ABBREVIATIONS

SERS	surface-enhanced Raman scattering
EM	electromagnetic
SPR	Surface plasmon resonance
AgNS	silver nanoshell
Ag NBS	silver nano-gap bumpy shell
RM	reporter molecule
NP	nanoparticle
PEG	poly(ethylene glycol)
NIR	near-infrared
UV	ultraviolet
TEOS	tetraethylorthosilicate
MPTS	3-mercaptopropyltrimethoxysilane
EG	ethylene glycol
PVP	poly(vinyl pyrrolidone)
4-CBT	4-chlorobenzenethiol
2-CBT	2-chlorobenzenethiol
2-FBT	2-fluorobenzenethiol

4-FBT	4-fluorothiophenol
4-BBT	4-bromobenzenethiol
DI water	deionized water
TEM	transmission electron microscope
HR-TEM	high resolution-transmission electron microscopy
Si NP	silica nanosphere
EGFR	epidermal growth factor receptor
HER2	human epidermal growth factor receptor 2

1. Introduction

1.1 The Advantages of SERS

Raman scattering is a vibrational emission of a unique spectral signature with narrow peaks, which is a strong point that provides detailed information about the structure of probe molecules. However, the use of this technique has been limited due to its extremely weak signal intensity. Surface enhanced Raman scattering (SERS) is a phenomenon that cause strong electromagnetic (EM) enhancement for molecules adsorbed on or near roughened metallic surfaces through collective oscillations of the metallic surface's electrons, surface plasmon resonance (SPR).[1]

As shown in Figure 1.1, when the metallic surface is irradiated by light, induced polarization generates large local EM fields on the particle. Firstly, the incident EM field, E_i, is enhanced due to the addition of the scattered field, $E_{i,s}$. It is caused by the particle polarization, yielding $E_i + E_{i,s}$ and exciting Raman modes on the probe molecule. Secondly, the emitted Raman field, E_R, can also polarize the metal nanoparticles and is enhanced by the addition of the scattered field, $E_{R,s}$, yielding $E_R + E_{R,s}$. The enhanced field $E_R + E_{R,s}$ increases the Raman intensity, I.[2] Through these mechanisms, SERS can gives strongly enhanced signals by a factor

of 10^{10} ~ 10^{15} compared to normal Raman scattering.[3]

SERS has numerous advantages over fluorescence as a spectroscopic tool, including high sensitivity,[4] narrow band width,[5] unique spectroscopic fingerprints of molecules and multiplex capacity,[6] non-photobleaching[7] and absence of interference from water.[8] Therefore, SERS has attracted much attentions as an alternative for fluorescence in various research fields, such as molecular detection,[9] diagnosis,[10] and bio-imaging[11] since SERS was first reported in 1970s.[12]

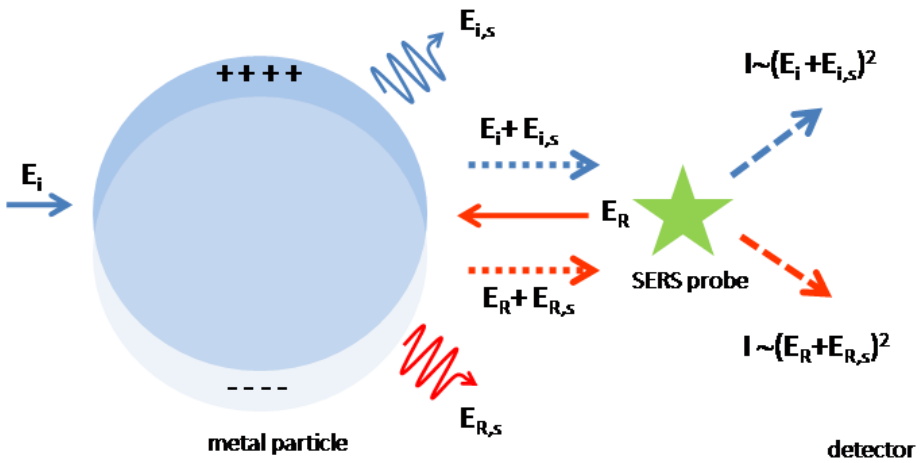

Figure 1.1 Schematic representation of the electromagnetic enhancement mechanism of SERS.[2]

1.2 Metallic Nanostructures and Signal Enhancement in SERS

Metallic nanostructure plays an important role in SERS because it can be designed to tune their SPR depending on their shape, size, and chemical composition (Figure 1.2).[13] There have been continuous studies on various metallic nanostructures such as metal nanorod[4, 14] nanocube,[15] and nanoshell,[16] whose plasmon resonance can be varied from visible to infrared region.

In addition, it is well known that the SERS activities for certain nanostructures largely depend on the effect of 'hot spot'.[17] 'Hot spot' is the localized areas of intense local EM field enhancement due to SPR and provides signal enhancements of up to 10^{15} orders of magnitude to the Raman signals. In this regard, the geometrical control of metal nanostructures is desirable for the creation of nano-gap junctions between adjacent metal NPs, which could induce strong optical field enhancement leading to make 'hot spot'.[18] Several results have been reported to make nano-gap junctions or aggregates using Ag or Au NPs to regulate the formation of 'hot spots'.[19] For example, Xia *et al* have reported SERS-active dimers of Ag NPs, which have the nano-sized gap (Figure 1.3). As-prepared Ag NP-dimer showed highest SERS

enhancement compared with the single nanosphere.[20] Therefore, it is important to control both metallic nanostructures and their surface geometry for strong enhancement of Raman signal.

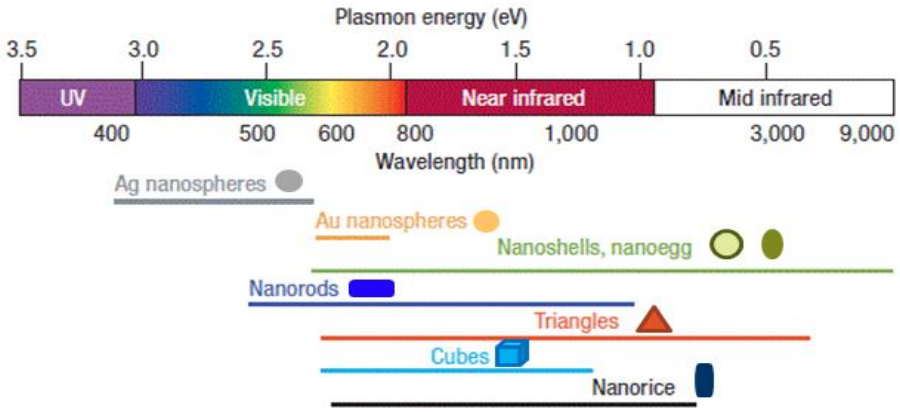

Figure 1.2 A range of plasmon resonances for a variety of nanoparticle morphologies.[13]

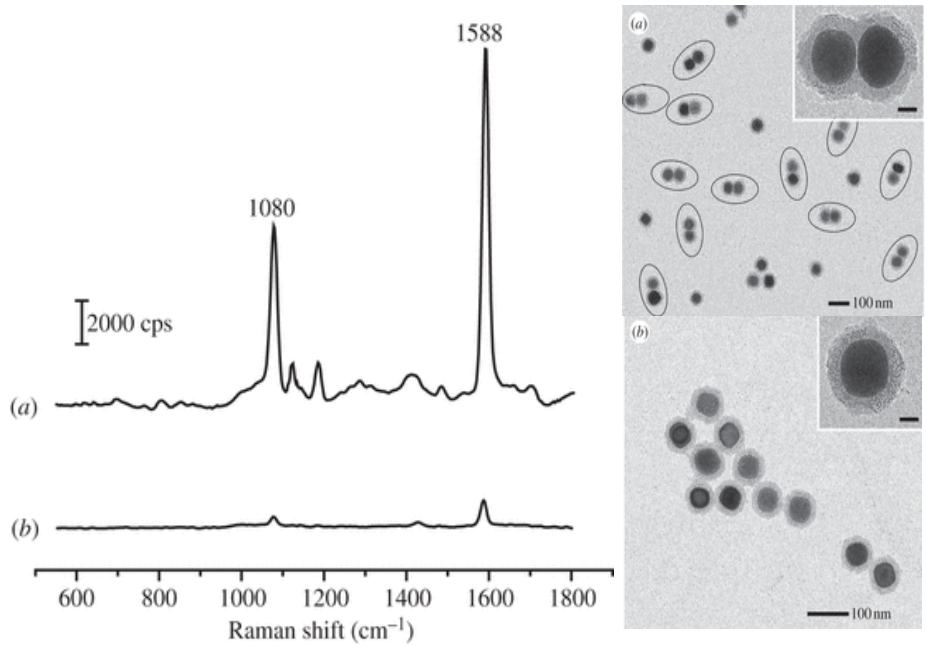

Figure 1.3 SERS spectra recorded from individual SERS substrate; (a) Ag NP-dimer, (b) single Ag NPs. [22]

1.3 SERS Tags in Bio-applications

SERS tags, which are composed of metal nanostructures and characteristic RMs, can provide specific Raman signals.[21] Recently, SERS tags have been successfully used for bio-appilcations.[20, 22] As shown in Figure 1.4, SERS tags are usually conjugated with a specific antibody for the detection of biological target. SERS tags allow identification of target by generating their own unique spectra.[23]

SERS tags are typically prepared by multi-synthetic steps, as shown in Figure 1.5. Metal nanostructures designed to ensure strong signal enhancement are prepared as SERS substrate, followed by coding procedure with RMs to give specific Raman signals. Ideal SERS tags should provide large SERS signals with reproducibility and stability, and should be easily synthesized.

However, SERS tags usually lacks stability, and the signal is easily disturbed by surrounding environment. Therefore, additional protecting step for SERS tag such as silica encapsulation and PEG coating is necessary. This encapsulation helps in providing biocompatibility, physical robustness, long-term stability.[20,24] Also, it provides surface modification site to SERS tags so that they can be easily functionalized with various receptor moieties for specific and active in vivo targeting of

biomarkers and reduces a chance for nonspecific binding and aggregation.

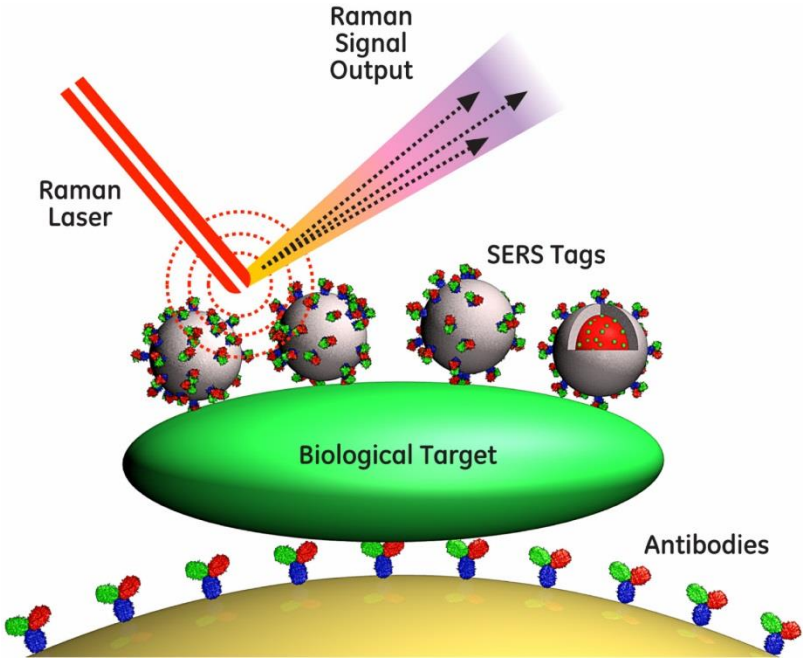

Figure 1.4 Diagram of the SERS-Tag based sandwich immunoassay.[23]

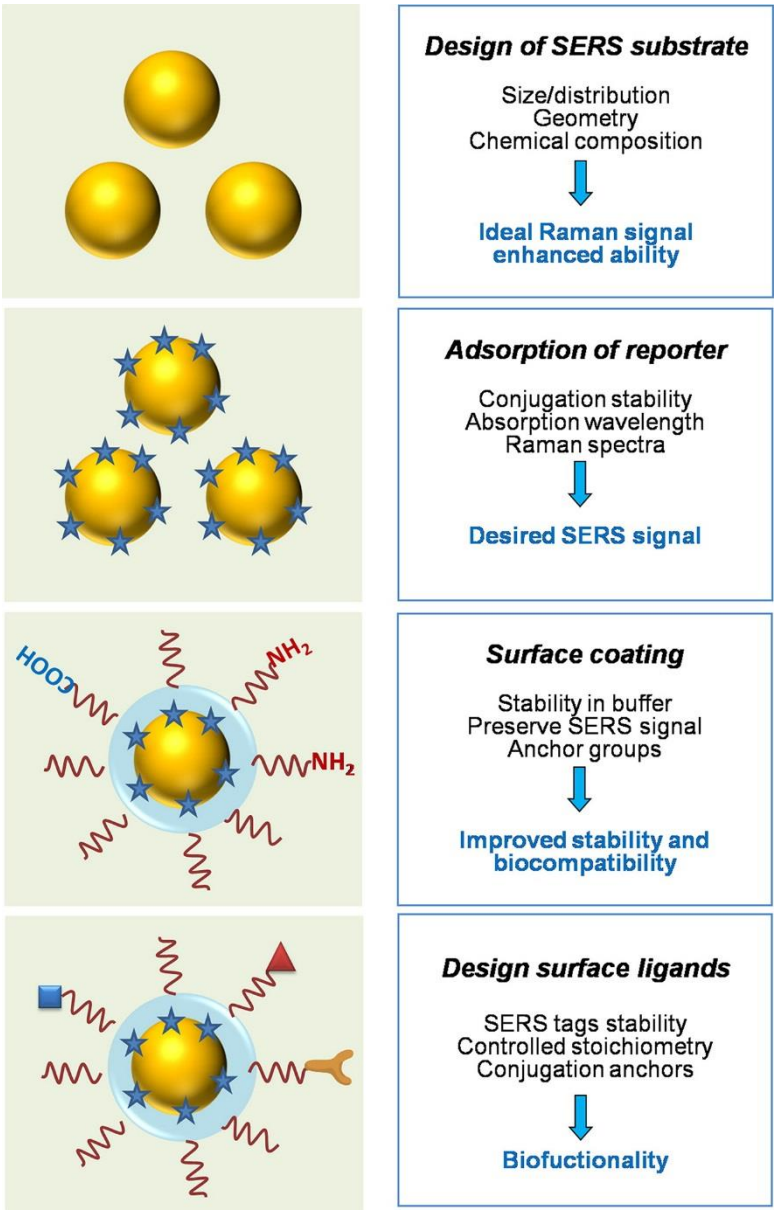

Figure 1.5 General steps of engineering SERS tags for bio-applications.[21]

1.4 Previous Study

Metal nanoshells (NSs), which consist of a dielectric core and a metallic shell, have gained a lot of attention due to their outstanding optical properties. The SPR of metal NSs can be controlled to a desired wavelength from the visible to infrared region by variation of the core size and thickness of the metallic shell layer. Among the diverse metal NSs for SERS, Ag and Au NSs are mostly often used as SERS substrates due to their strong EM field enhancement. In particular, Ag can generate 10 to 1000-fold greater Raman signal than Au.[25] Previously, single-step synthesis of Ag NSs and their applications to *in vivo* cell tracking[26] and detection of pesticide[27] were reported by our group. During the Ag NSs synthesis, we found that a complete layer of Ag shells was quite rapidly formed onto silica nanoparticles (Si NPs) within 2 min. The thickness of Ag NSs was effectively controlled and increased by increasing the concentration of Si NPs, which resulted in a shift of plasmon resonance from the visible to the near-infrared (NIR) region. This rapid growth of Ag NSs was attributed to an increase in the reduction potential of the Ag^+ ions in ethylene glycol, which led to facile reduction of the Ag^+ ions by octylamine even at room temperature. As-prepared Ag NSs exhibited a highly enhanced Raman signal. Especially, Ag NSs could be synthesized

with high reproducibility, and showed no significant toxicity *in vivo*. Although afore mentioned characteristics allow Ag NSs as a suitable candidate for SERS tag, additional RM attachment step is still needed to prepare Ag NSs based SERS tags. (Figure 1.6)

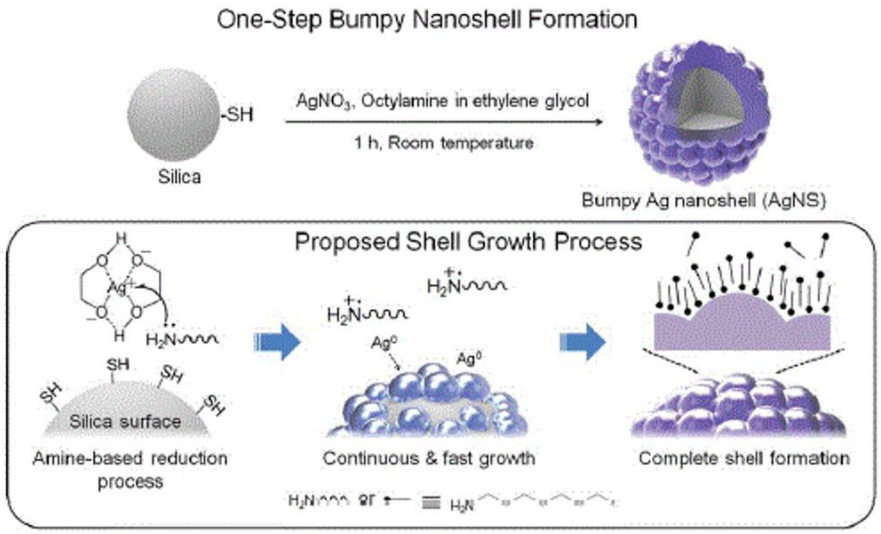

Figure 1.6 Schematic illustration of a seedless and single step synthesis of Ag NS with bump-structures on its surface via reduction of Ag^{+} ion by octylamine in ethylene glycol solution.[26]

1.5 Research Objectives

In the present work, in-depth study was performed on the synthesis of SERS tags having both nano-gap and highly enhanced unique Raman signals via a single-step method. Being different from typical fabrication method of SERS tags which requires additional introduction step of Raman RMs to metal nanostructure, Ag nano-gap bumpy shell based SERS tags (Ag NBS) were prepared by one-pot procedure. Ag NBSs exhibited highly enhanced Raman signal compared to the one from Ag NSs based SERS tag. In addition, we demonstrate the potential of two kinds of Ag-NBSs on duplex-imaging of cancer cells, which overexpress unique receptors on the surface.

2. Experimental Section

2.1 Chemicals and Materials

Tetraethylorthosilicate (TEOS), 3-mercaptopropyl trimethoxysilane (MPTS), ethylene glycol (EG), poly(vinyl pyrrolidone) (PVP), octylamine (OA), silver nitrate (AgNO3, 99.99+%), *N*-hydroxysuccinimide (NHS), *N*-(3-dimethylaminopropyl)-*N*'-ethylcarbodiimide hydrochloride (EDC), 2-chlorobenzenethiol (2-CBT), 4-chlorobenzenethiol (4-CBT), 4-bromobenzenethiol (4-BBT), 2-fluorobenzenethiol (2-FBT) and 4-fluorobenzenethiol (4-FBT) were purchased from Sigma-Aldrich Inc. and used without further purification. Ammonium hydroxide (NH_4OH, 27%) and ethanol (98%) were provided by Daejung chemical (Busan, Korea). Poly(ethylene glycol)-2-mercaptoethyl ether acetic acid (HOOC-PEG-SH, Mw 5,000) was purchased from Creative PEG Works (Winston Salem, NC, USA). EGFR and HER2 antibodies were purchased from Santa Cruz Biotechnology (Santa Cruz, CA, USA). Deionized (DI) water was used for all the experiments.

2.2 Instruments

Absorption spectra of Ag NBS were measured using a UV spectrometer (Optizen 2120UV, Mecasys). The morphology and the size of Ag NBS were characterized using transmission electron microscope (TEM, LIBRA 120, Carl Zeiss). The SERS spectrum was recorded with portable-Raman system (B&W TEK, i-Raman) and confocal Raman microscope system (JY-Horiba, LabRam300) which is equipped with a diode laser emitting at 785 nm.

2.3 Preparation of Thiol-functionalized Silica NPs (Si NPs)

A 1.6 mL tetraorthosilicate (TEOS) was added to 40 mL of absolute ethanol. Then, 3.0 mL ammonium hydroxide (28 wt % in water) was added to the TEOS solution. The mixture was sonicated for 4 h at room temperature. The resulting silica colloids were centrifuged and washed with ethanol several times. To obtain thiol-modified silica sphere, 150 uL of MPTS and 30 uL of ammonium hydroxide were added to the well-dispersed silica colloids (3.0 mL, 50 mg silica NP mL^{-1} ethanol). Then, the mixture was mixed with a magnetic stirring bar for 4 h at room temperature. The resulting thiol-functionalized Si NPs were centrifuged and washed with ethanol several times.

2.4 Fabrication of Ag Nano-gap Bumpy Shells (Ag NBSs)

To synthesize Ag NBS, 29.73 mg of $AgNO_3$ was added to 25 mL of ethylene glycol (EG) and 5 mg of PVP were added to 25 mL EG. Well-dispersed thiol-functionalized Si NPs (50mg NPs mL^{-1} ethanol) were added in PVP solution (in EG). $AgNO_3$ solution (in EG) was added in the mixture. Then, 41.31 uL of octylamine was added to the mixture. After 60 s, Raman RMs were added and stirred for 1 h at room temperature. The resulting Ag NBSs were centrifuged and washed with ethanol several times to remove excess reagents.

2.5 Preparation of Antibody-conjugated Ag NBSs

In order to give biocompatibility and introduce functional groups, the Ag NBSs surface was coupled with a heterofunctional PEG. For conjugation with EGFR and HER2 antibody, each of Ag NBSs$_{[4\text{-}FBT]}$ and Ag NBSs$_{[2\text{-}FBT]}$ surface was modified with HOOC-PEG-SH (2 mM in ethanol). The HOOC-PEG-coated Ag NBSs$_{[4\text{-}FBT]}$ and Ag NBSs$_{[2\text{-}FBT]}$ dispersions were washed with ethanol several times by centrifugation and resuspension in 0.1 M of phosphate buffered saline (PBS, 7.0). After activation of the carboxylic group of Ag NBSs$_{[4\text{-}FBT]}$ and Ag NBSs$_{[2\text{-}FBT]}$ with 2 mM of EDC and 5 mM of NHS in 0.1 M of PBS (pH 6.0), 20 μg portion of the antibody was added to pre-activated PEGylated Ag NBSs$_{[4\text{-}FBT]}$ and Ag NBSs$_{[2\text{-}FBT]}$ dispersion. The mixture was shaken for 2 h at room temperature. Each of EGFR antibody conjugated Ag NBSs$_{[4\text{-}FBT]}$ (EGFR-Ag NBSs$_{[4\text{-}FBT]}$) and HER2 antibody conjugated Ag NBSs$_{[2\text{-}FBT]}$ (HER-Ag NBSs$_{[2\text{-}FBT]}$) was rinsed with 0.1 M of PBS (pH 7.0) several times.

2.6 Cell Preparation

A549 (adenocarcinomic human alveolar basal epithelial cell line) and H522 cell line (human nonsmall cell lung cancer cell line) were obtained from Korean cell line bank (Seoul, Korea). A549 cell line was grown in F-12 complete medium and H522 cell line was grown in RPMI-1640 complete medium. The complete media for A549 and H522 cell lines were supplemented with 10% fetal bovine serum and 1% penicillin/streptomycin (GibcoBRL, Grand Island, NY, USA). The cells were incubated at 37 ℃ in a humidified atmosphere containing 5% CO_2. The cells were seeded into 20000 cells in 300 μl media per well on Labteck 8 well slide chamber. They were incubated overnight at 37 ℃ in a humidified atmosphere containing 5% CO_2. Next day, they were washed with sterile PBS and fixed with 4% paraformaldehyde for 15 minutes. Then, they were washed with sterile PBS again and incubated with 5% BSA for 1 hr. Each well was treated 15 μg of Ab conjugated Ag NBSs (1 mg mL^{-1}). A549 cell lines were treated with EGFR-Ag $NBS_{[4\text{-}FBT]}$ and H522 cell lines were treated with HER2-Ag $NBS_{[2\text{-}FBT]}$ for 2 h at room temperature. Then, they was rinsed with 0.1 % TPBS for several times, 0.1 M PBS (pH 7.0) for several times, and DI for several times.

2.7 SERS Measurement

SERS mapping of individual cancer cells was performed using a confocal Raman microscope system (JY-Horiba, LabRam300). SERS mapping was conducted using a 785 nm laser excitation with a power of 7.5 mW and an acquisition times of 1 s.

3. Results and Discussion

3.1 Characteriztion of Ag NBSs

Ag NBSs were synthesized as shown in Figure 3.1. Silica NPs (Si NPs) were used as a dielectric core due to their ease of functionalization and synthesis. First, uniform sized Si NPs (150 nm) were obtained by Stöber method[28] and functionalized with thiol group to introduce Ag NPs onto the surface of Si NPs. The thiol-functionalized Si NPs were then mixed with 3.5 mM of $AgNO_3$, 5 mM of octylamine as a reducing agent, poly-(vinylpyrrolidone) (PVP) as a stabilizer in ethylene glycol. After 1 min, various amounts of Raman RMs were added into the mixture. Ag NBSs, which was synthesized by using 4-fluorobenzenthiol (4-FBT) as a Raman RMs, is denoted as Ag $NBSs_{[4\text{-}FBT]}$. The Ag $NBSs_{[4\text{-}FBT]}$ were characterized by transmission electron microscopy (TEM), UV/Vis spectrophotometer and Raman spectroscopy. Figure 3.2a shows the TEM image of the Ag $NBSs_{[4\text{-}FBT]}$, which showed uniformity of synthesized particles with a diameter of 250 nm. Furthermore, Ag $NBSs_{[4\text{-}FBT]}$ showed a bumpy structure which can create ‘hot spots’ that induce a strong EM field enhancement compared with smooth surfaces. To confirm the existence of nano-gap on metallic surface, Ag $NBSs_{[4\text{-}FBT]}$ were observed with high resolution-transmission electron microscopy

(HR-TEM). As shown in Figure 3.2b, nano-gap were created on the surface of Ag NBSs and the size of gap was 2 nm in average. Figure 3.2c, d shows the absorbance spectra and typical SERS signals of Ag NBSs$_{[4\text{-}FBT]}$. Previously reported Ag NSs showed distinct absorption band in NIR region arising from its complete metallic shell structure.[26] On the other hand, Ag NBSs exhibited broad absorbance ranging from visible to NIR region as Ag NBSs have nano-gap structure between Ag NPs affording Ag NPs a coalesced network-like structure.[29] This broad absorption is beneficial to an effective excitation of Ag NBSs using any laser lines. Figure 3.3a shows the linear correlation between the peak intensity at 1075 cm^{-1} and the concentration of Raman RMs. The intensity was increased with increasing the added amount of Raman RMs. However, small Ag NPs were also produced at concentrations of Raman RMs higher than 0.5 mM, which resulted in large aggregates of Ag NPs, as shown in Figure 3.3b. Therefore, under the condition of Ag NPs not forming aggregation, the optimal concentration of Raman RMs was identified as 0.5 mM.

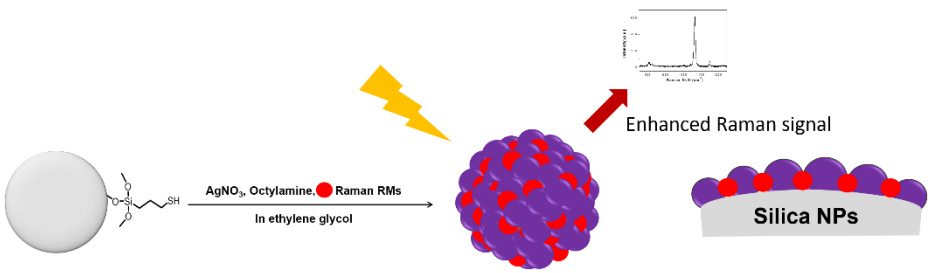

Figure 3.1 Schematic illustration of Ag-NBS synthesis.

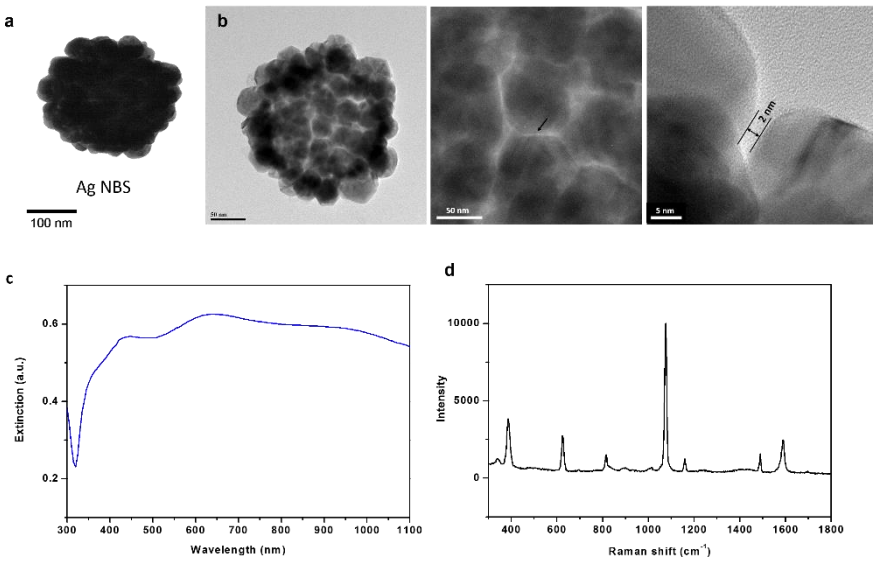

Figure 3.2 Characterization of Ag NBSs. (a) TEM image and (b) UV/Vis extinction spectrums of Ag NBSs$_{[4\text{-FBT}]}$ (c) SERS spectrum of 4-FBT on Ag NBSs$_{[4\text{-FBT}]}$ with the 785 nm photo-excitation of 30 mW laser power and light acquisition time of 1 s.

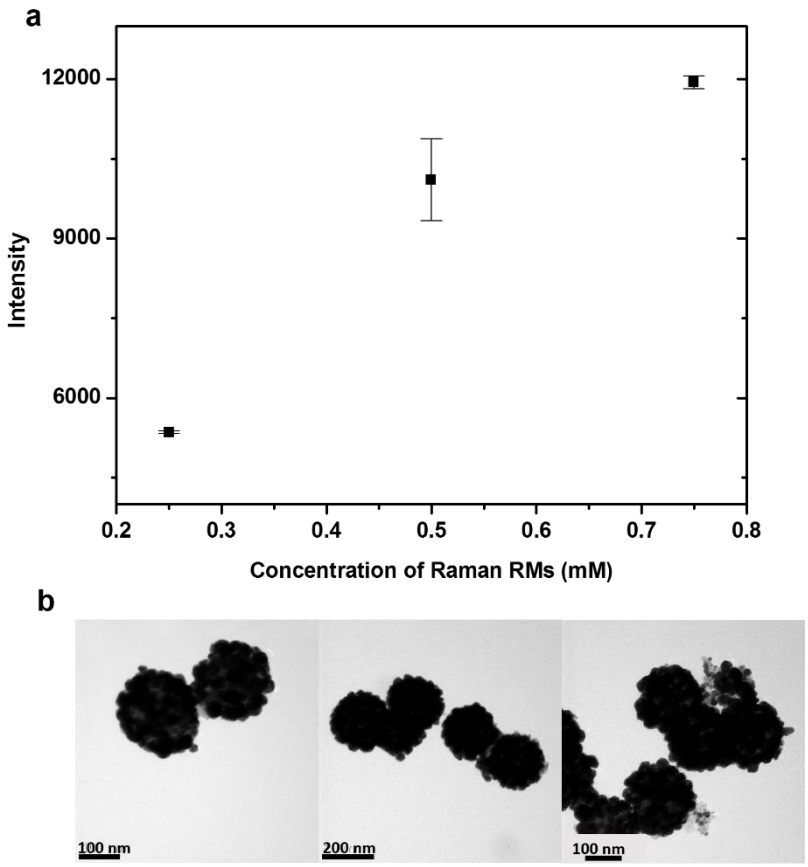

Figure 3.3 Effect of concentration of Raman RMs. (a) correlation between RM concentrations and SERS intensity of Ag $NBSs_{[4\text{-}FBT]}$ at 1075 cm^{-1}, (b) TEM images of Ag $NBSs_{[4\text{-}FBT]}$ with different concentarion of 4-FBT; 0.25 mM, 0.5 mM, 0.75 mM from left to right. SERS spectra were obtained using a 785 nm laser with 30 mW power.

3.2 Kinetics of Ag NBSs Formation

The kinetics for the formation of Ag NBS was investigated by TEM and UV/Vis spectrophotometer at each time interval (10, 60, 90, 120, 240, 360, 600, and 3600s) during 1 h reaction time. (Figure 3.4a, b) The rapid formation of Ag NBSs was confirmed by plasmon absorption, which clearly corresponded to the structure of Ag NBSs as shown in the TEM images. After adding octylamine as a reducing agent, small size Ag NPs began to be introduced on the surface of Si NPs and continued to grow as a function of reaction time until 60 s. The absorption peaks between 400 and 500 nm were also growing, which corresponded to the structure with separated Ag NPs on the surface. Then, Ag NPs embedded Si NPs were surrounded by networks including Ag NPs due to the addition of Raman RM with the absorption peaks between 350 and 400 nm. Depending on elapsed time, Ag NPs in networks were gradually increased onto Si NPs, resulting in the formation of Ag NBSs after 1 h. The absorbance peaks were gradually shifted to NIR region, and finally distinct peaks disappeared, indicating that Ag NBSs were formed with coalesced network-like structure. As shown in Figure 3.4c, the color of Ag NBS dispersion was changed from light yellow to black. According to the results of the kinetic study, Ag NPs were generated on the surface

of thiol-functionalized Si NPs in the presence of Raman RMs, and the nano-gap structure was induced by embedding of Raman RMs between Ag NPs structures on silica surface. Therefore, additional experiments were conducted to investigate the effect of size of Raman RMs. Ag NBSs were synthesized by using three kinds of PEG-SH with different molecule size. Figure 3.4d-f shows TEM images of Ag NBS obtained by using PEG 2000, PEG 5000, PEG 10000. As the molecular weight of PEG increased, the prepared Ag NBSs showed more large-sized gap between Ag NPs on the surface of Si NPs. This result indicates that the added RMs are trapped between Ag NPs, and the gap distance between Ag NBSs was increased as the size of RMs was increased.

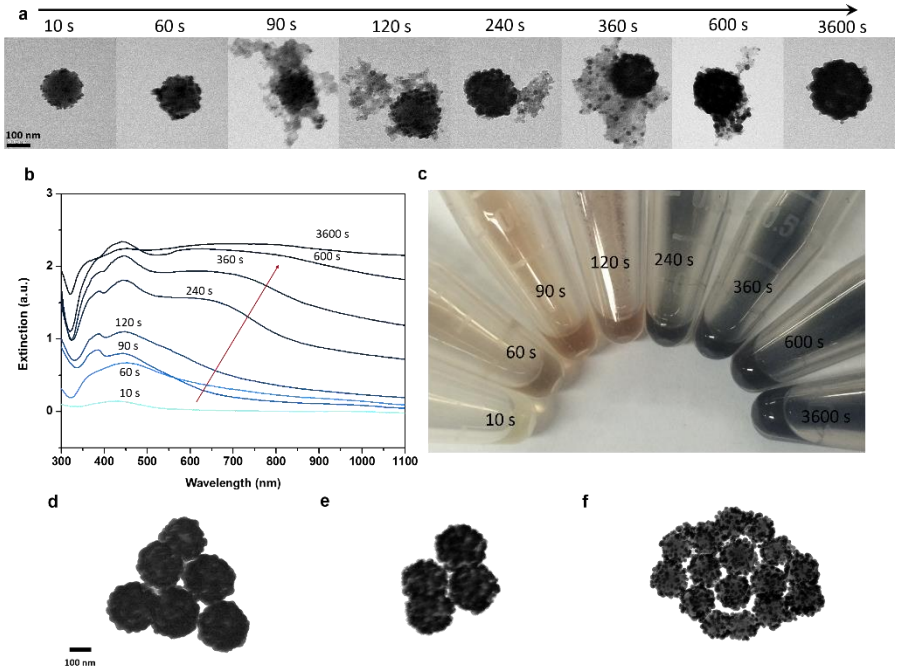

Figure 3.4 Kinetics of the formation of Ag nano-gap bumpy shells (Ag NBSs). (a) TEM images and (b) UV/Vis extinction spectra of growing Ag NBSs during the reaction, 10 s, 60 s. 90 s, 120 s, 240 s, 360 s, 600 s and 3600 s, respectively. (c) Photograph of Ag NBSs solution at various reaction times, showing the change in color. TEM images of Ag NBSs obtained with (d) PEG (MW 2,000), (e) PEG (MW 5,000), and (f) PEG (MW10,000).

3.3 SERS Signal Enhancement and Stability of Ag NBSs

To compare the SERS intensity of Raman RMs trapped in Ag NBS and just adsorbed on to the surface of Ag NSs, Raman signals of them were measured. Although Ag NSs were treated with higher concentration of Raman RMs (20 mM) than the one of Ag NBS (0.5 mM), Raman intensity of Ag NBSs were 3.5 times stronger than the one of Ag NSs as shown in Figure 3.5. This is due to the structural benefit of Ag NBS having RMs trapped in nano-gap rather than on the surface. Figure 3.5 shows the stability of Ag NBSs and Ag NSs. To investigate the stability of Ag NBS, Raman intensity of Ag NBSs was measured after 4 weeks. Compare to the ones right after the synthesis, the signal intensity of Ag NBS was decreased by 5.5 %, whereas that of Ag NS was decreased by 45 % after 4 weeks. Ag NBSs showed relatively excellent stability than Ag NSs because Raman RMs were trapped in nano-gap of Ag NBSs.

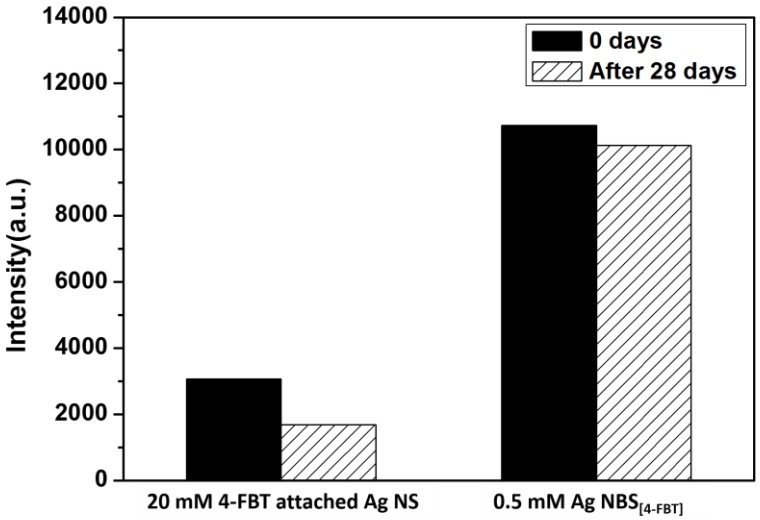

Figure 3.5 Comparison of SERS intensity and signal stability between Ag $NSs_{[4\text{-}FBT]}$ and Ag $NBSs_{[4\text{-}FBT]}$.SERS signals were obtained with the 785 nm photo-excitation of 30 mW laser power and light acquisition time of 1 s.

3.4 Multiplexing Capability of Ag NBSs

The characteristic peaks of Raman RMs can offer multiplexing capability. As shown in Figure 3.6, various kind of Ag NBSs were synthesized using different Raman RMs such as 2-chlorobenzenethiol (2-CBT), 4-chlorobenzenethiol (4-CBT), 4-bromobenzenethiol (4-BBT), 2-fluorobenzenethiol (2-FBT) and 4-FBT. SERS spectra were analyzed under 785 nm laser and evaluated their multiplexing capability. Each Ag NBSs had its own characteristic Raman spectra: 348, 427, 470, 732, 1039, 1107 and 1570 cm^{-1} for Ag $NBSs_{[2\text{-}CBT]}$, 343, 540, 1069, 1099 and 1569 cm^{-1} for Ag $NBSs_{[4\text{-}CBT]}$, 492, 1071 and 1565 cm^{-1} for Ag $NBSs_{[4\text{-}BBT]}$, 386, 494, 470, 1027, 1062, 1119, 1223, 1469 and 1591 cm^{-1} for Ag $NBSs_{[2\text{-}FBT]}$, 386, 623, 1075 and 1589 cm^{-1} for Ag $NBSs_{[4\text{-}FBT]}$, which are easy to be distinguished from the mixed signals in a multiplex detection system.

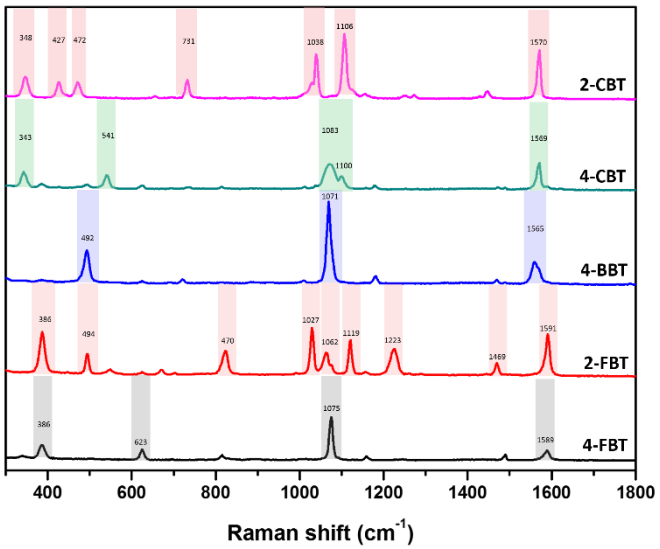

Figure 3.6 Multiplexing capability of Ag NBSs. SERS spectra of Ag NBS trapped simple aromatic compounds such as 2-CBT, 4-CBT, 4-BBT, 2-FBT and 4-FBT were obtained with the 785 nm photo-excitation of 30 mW laser power and light acquisition time of 1 s.

3.5 *In vitro* SERS Imaging of Cancer Cells

A549 and H522 cell lines, that are lung cancer cell lines, were used as the imaging target for SERS tags. It has been reported that A549 cell lines overexpress EGFR and H522 overexpress HER2 receptor.[30] Antibodies corresponding to EGFR and HER2 were conjugated onto Ag $NBSs_{[4\text{-}FBT]}$ and Ag $NBSs_{[2\text{-}FBT]}$, respectively. EGFR-Ag $NBSs_{[4\text{-}FBT]}$ and HER2-Ag $NBSs_{[2\text{-}FBT]}$ were incubated with A549 or H522 cell lines for 2 h to allow active targeting. Using the characteristic SERS signals of Raman RMs as a signature of specific biomarker proteins, SERS mapping for the expressed cancer biomarkers were obtained using a confocal Raman microscope. Figure 3.7a-d show bright filed microscope images of each cells and Figure 3.7e-h show SERS mapping for each cells, Figure 3.7i-j show merged images between bright field and SERS mapping, and Figure 3.7m-p show the corresponsive SERS spectra observed from each cells. From SERS mapping, the SERS intensities at 623 cm^{-1} and 494 cm^{-1} corresponds to 4-FBT and 2-FBT that were used to distinguish two biomarker. Figure 3.7a, e, i and b, f, j show the SERS mapping of 4-FBT of EGFR-Ag $NBS_{[4\text{-}FBT]}$ treated EGFR-positive A549 and EGFR-negative H522 cells (green signal). EGFR-Ag $NBS_{[4\text{-}FBT]}$ targeted only A549 cell lines, showing SERS signal from A549 cell lines

at 623 cm^{-1} peak of 4-FBT (Figure 3.7a, e, i, m). There was no 4-FBT signal from H522 cells (Figure 3.7b, f, j, n). As expected, in the case of HER2-Ag $NBSs_{[2\text{-}FBT]}$, the same result was obtained. Figure 3.7c, g, k, o and d, h, i, p show the SERS mapping of 2-FBT of HER2-Ag $NBS_{[2\text{-}FBT]}$ treated HER2-positive H522 and HER2-negative A549 cell lines (purple signal). HER2-Ag $NBSs_{[2\text{-}FBT]}$ targeted only H522 cell lines and SERS signal was detected at 494 cm^{-1} of 2-FBT (Figure 3.7k, l, o, p). When H522 cell lines were treated with EGFR-Ag $NBSs_{[4\text{-}FBT]}$ and HER2-Ag $NBSs_{[2\text{-}FBT]}$ simultaneously, only HER2-Ag $NBSs_{[2\text{-}FBT]}$ targeted H522 cell lines and Raman signals of 2-FBT was observed, as shown in Figure 3.8. These results clearly indicate that Ag NBSs could be used as multiplex-capable SERS tags in bio-imaging with strong signal.

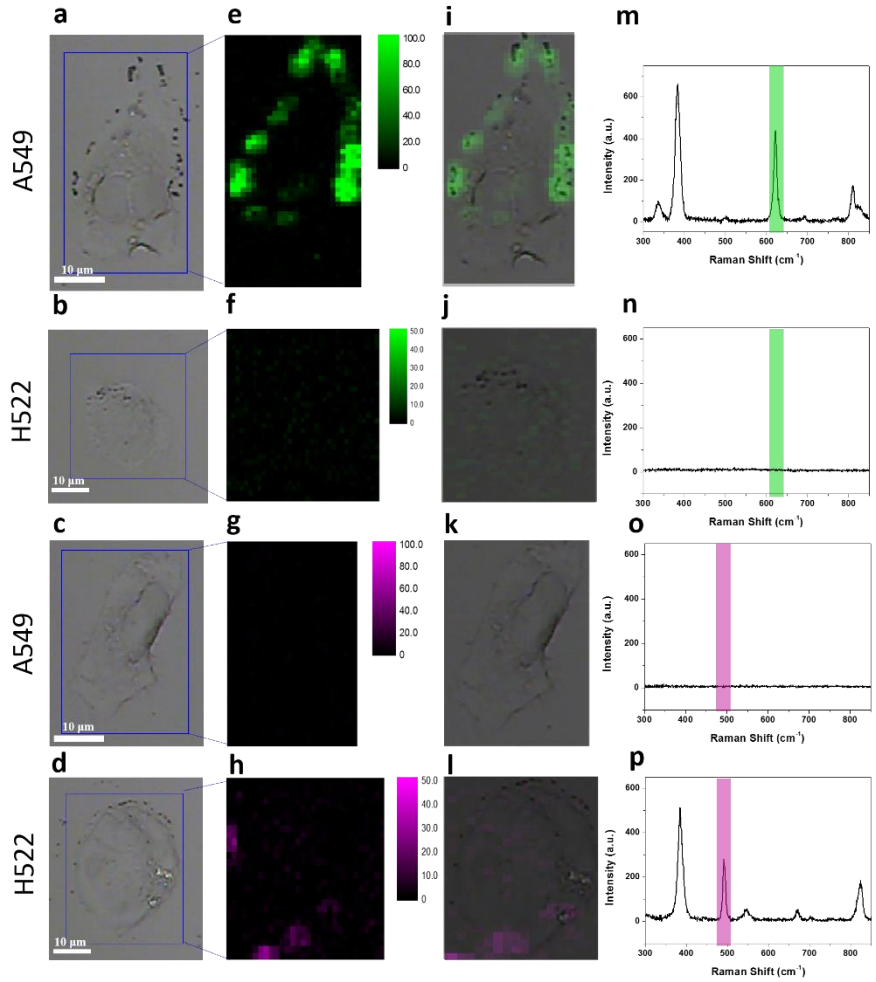

Figure 3.7 (a)-(d) Bright field images for two different types of lung cancer cell lines, A549 and H522. A549 cell lines were treated (a),(e),(i),(m) EGFR-Ag $NBSs_{[4\text{-}FBT]}$ and (c),(g),(k),(o) HER2-Ag $NBSs_{[2\text{-}FBT]}$. H522 cell lines were treated (b),(f),(j),(n) EGFR-Ag $NBSs_{[4\text{-}FBT]}$ and (d),(h),(l),(p) HER2-Ag $NBSs_{[2\text{-}FBT]}$. SERS mapping of corresponding cell lines were measured at (e),(f) 623 cm^{-1} (4-FBT)

displayed in green and at (g),(h) 494 cm^{-1} (2-FBT) displayed in purple. (i)-(l) Merged SERS mapping images, (m)-(p) SERS spectra of A549 and H522 cell lines using the 785 nm photo-excitation of 7.5 mW laser power and light acquisition time of 1 s.

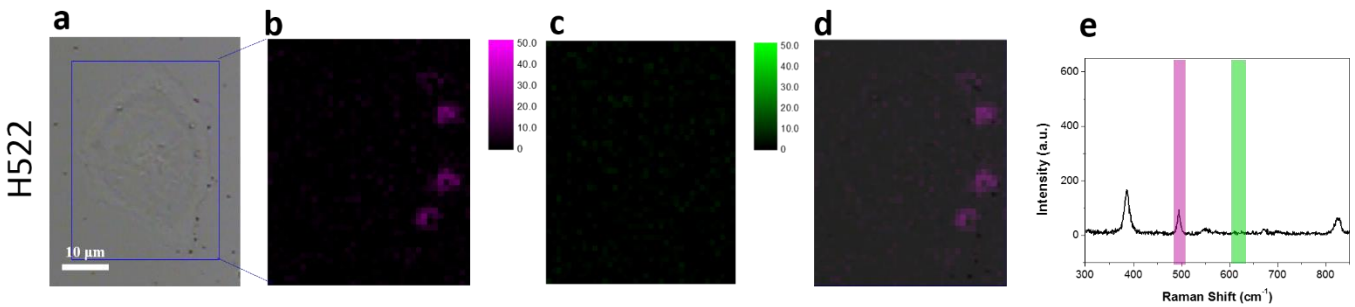

Figure 3.8 H522 cell lines were treated with a mixture (EGFR-Ag NBSs$_{[4\text{-FBT}]}$ and HER2-Ag NBSs$_{[2\text{-FBT}]}$). (a) Bright field images for H522 cell lines. SERS mapping of corresponding cell lines were measured at (b) 494 cm^{-1} (2-FBT) displayed in purple and at (c) 623 cm^{-1} (4-FBT) displayed in green. (d) Merged SERS mapping, (e) SERS spectra of H522 cell lines were obtained using the 785 nm photo-excitation of 7.5 mW laser power and light acquisition time of 1 s.

Conclusions

Raman RMs trapped Ag NBSs were synthesized via single-step method, which have bumpy and nano-gap structure. An important finding is that the nano-gap was formed when small Raman RMs were caught between Ag NPs. The resulting Ag NBSs generated strong SERS signals with high reproducibility and showed much better stability than the ones with Raman RMs adsorbed on the surface of Ag NSs. The signal intensity of the prepared Ag NBSs could be enhanced due to the nano-gap between the Ag NPs. Using various Raman RMs, diverse SERS tags were synthesized showing each own characteristics signals with multiplex capability. Furthermore, Ag NBSs conjugated with specific antibodies were used as SERS-based bio-imaging nanoprobes. Two different Ag NBSs showed distinguishable strong SERS signal, and could specifically recognize the targeting cells, thereby demonstrating their potential for use as a SERS tag for bio-imaging.

References

1. Moskovits, M., Surface-enhanced spectroscopy. *Reviews of modern physics* **1985,** *57* (3), 783.

2. Contreras-Cáceres, R.; Sierra-Martín, B.; Fernández-Barbero, A., *Surface-Enhanced Raman Scattering Sensors based on Hybrid Nanoparticles*. 2011.

3. Kneipp, K.; Kneipp, H.; Dresselhaus, M. S.; Lefrant, S., Surface–enhanced Raman scattering on single–wall carbon nanotubes. *Philosophical Transactions of the Royal Society of London. Series A: Mathematical, Physical and Engineering Sciences* **2004,** *362* (1824), 2361-2373.

4. Chaney, S. B.; Shanmukh, S.; Dluhy, R. A.; Zhao, Y.-P., Aligned silver nanorod arrays produce high sensitivity surface-enhanced Raman spectroscopy substrates. *Applied Physics Letters* **2005,** *87* (3), 031908.

5. Kneipp, K.; Kneipp, H.; Itzkan, I.; Dasari, R. R.; Feld, M. S., Surface-enhanced Raman scattering and biophysics. *Journal of Physics: Condensed Matter* **2002,** *14* (18), R597.

6. Cao, Y. C.; Jin, R.; Mirkin, C. A., Nanoparticles with Raman spectroscopic fingerprints for DNA and RNA detection. *Science* **2002,** *297* (5586), 1536-1540.

7. Jun, B.-H.; Noh, M. S.; Kim, G.; Kang, H.; Kim, J.-H.; Chung, W.-J.; Kim, M.-S.; Kim, Y.-K.; Cho, M.-H.; Jeong, D. H., Protein separation and identification using magnetic beads encoded with surface-enhanced Raman spectroscopy. *Analytical biochemistry* **2009,** *391* (1), 24-30.

8. Vankeirsbilck, T.; Vercauteren, A.; Baeyens, W.; Van der Weken, G.; Verpoort, F.; Vergote, G.; Remon, J. P., Applications of Raman spectroscopy in pharmaceutical analysis. *TrAC trends in analytical chemistry* **2002,** *21* (12), 869-877.

9. Liu, H.; Zhang, L.; Lang, X.; Yamaguchi, Y.; Iwasaki, H.; Inouye, Y.;

Xue, Q.; Chen, M., Single molecule detection from a large-scale SERS-active Au79Ag21 substrate. *Scientific reports* **2011,** *1*.

10. (a) Sha, M. Y.; Xu, H.; Penn, S. G.; Cromer, R., SERS nanoparticles: a new optical detection modality for cancer diagnosis. *Nanomedicine* **2007,** *2* (5), 725-734; (b) Neng, J.; Harpster, M. H.; Wilson, W. C.; Johnson, P. A., Surface-enhanced Raman scattering (SERS) detection of multiple viral antigens using magnetic capture of SERS-active nanoparticles. *Biosensors and Bioelectronics* **2013,** *41*, 316-321.

11. Liu, X.; Knauer, M.; Ivleva, N. P.; Niessner, R.; Haisch, C., Synthesis of Core− Shell Surface-Enhanced Raman Tags for Bioimaging. *Analytical chemistry* **2009,** *82* (1), 441-446.

12. Fleischmann, M.; Hendra, P. J.; McQuilan, A. J., RAMAN SPECTRA OF PYRIDZNE ADSORBED AT A SILVER ELECTRODE. *Chemical Physics Letters* **1974,** *26*.

13. Lal, S.; Link, S.; Halas, N. J., Nano-optics from sensing to waveguiding. *Nature photonics* **2007,** *1* (11), 641-648.

14. Zhu, Y.; Kuang, H.; Xu, L.; Ma, W.; Peng, C.; Hua, Y.; Wang, L.; Xu, C., Gold nanorod assembly based approach to toxin detection by SERS. *J. Mater. Chem.* **2012,** *22* (6), 2387-2391.

15. Kodiyath, R.; Malak, S. T.; Combs, Z. A.; Koenig, T.; Mahmoud, M. A.; El-Sayed, M. A.; Tsukruk, V. V., Assemblies of silver nanocubes for highly sensitive SERS chemical vapor detection. *Journal of Materials Chemistry A* **2013,** *1* (8), 2777-2788.

16. Hirsch, L. R.; Gobin, A. M.; Lowery, A. R.; Tam, F.; Drezek, R. A.; Halas, N. J.; West, J. L., Metal nanoshells. *Annals of biomedical engineering* **2006,** *34* (1), 15-22.

17. Wustholz, K. L.; Henry, A.-I.; McMahon, J. M.; Freeman, R. G.; Valley, N.; Piotti, M. E.; Natan, M. J.; Schatz, G. C.; Duyne, R. P. V., Structure− Activity Relationships in Gold Nanoparticle Dimers and Trimers for Surface-Enhanced Raman Spectroscopy. *Journal of the American Chemical Society* **2010,** *132* (31), 10903-10910.

18. Wei, H.; Xu, H., Hot spots in different metal nanostructures for

plasmon-enhanced Raman spectroscopy. *Nanoscale* **2013,** *5* (22), 10794-10805.

19. Lim, D.-K.; Jeon, K.-S.; Kim, H. M.; Nam, J.-M.; Suh, Y. D., Nanogap-engineerable Raman-active nanodumbbells for single-molecule detection. *Nature materials* **2009,** *9* (1), 60-67.

20. Xia, X.; Li, W.; Zhang, Y.; Xia, Y., Silica-coated dimers of silver nanospheres as surface-enhanced Raman scattering tags for imaging cancer cells. *Interface focus* **2013,** *3* (3), 20120092.

21. Wang, Y.; Yan, B.; Chen, L., SERS tags: novel optical nanoprobes for bioanalysis. *Chemical reviews* **2012,** *113* (3), 1391-1428.

22. Qian, X.; Peng, X.-H.; Ansari, D. O.; Yin-Goen, Q.; Chen, G. Z.; Shin, D. M.; Yang, L.; Young, A. N.; Wang, M. D.; Nie, S., In vivo tumor targeting and spectroscopic detection with surface-enhanced Raman nanoparticle tags. *Nature biotechnology* **2007,** *26* (1), 83-90.

23. Paxon, T. L.; Duthie, R. S.; Renko, C.; Burns, A.; Mondello, F. J.; Lesaicherre, M., Identifying biological agents with surface-enhanced Raman scattering. *SPIE Newsroom* 2011.

24. Huang, J.; Kim, K. H.; Choi, N.; Chon, H.; Lee, S.; Choo, J., Preparation of silica-encapsulated hollow gold nanosphere tags using layer-by-layer method for multiplex surface-enhanced Raman scattering detection. *Langmuir* **2011,** *27* (16), 10228-10233.

25. (a) Kneipp, K.; Kneipp, H.; Kneipp, J., Surface-enhanced Raman scattering in local optical fields of silver and gold nanoaggregates from single-molecule Raman spectroscopy to ultrasensitive probing in live cells. *Accounts of chemical research* **2006,** *39* (7), 443-450; (b) Kneipp, K.; Dasari, R. R.; Wang, Y., Near-infrared surface-enhanced Raman scattering (NIR SERS) on colloidal silver and gold. *Applied spectroscopy* **1994,** *48* (8), 951-955.

26. Kang, H.; Yang, J.-K.; Noh, M. S.; Jo, A.; Jeong, S.; Lee, M.; Lee, S.; Chang, H.; Lee, H.; Jeon, S.-J., One-Step Synthesis of Silver Nanoshell with Bumps for Highly Sensitive Near-IR SERS Nanoprobes. *Journal of Materials Chemistry B* **2014,** *2*, 4415-4421.

27. Yang, J.-K.; Kang, H.; Lee, H.; Jo, A.; Jeong, S.; Jeon, S.-J.; Kim, H.-I.; Lee, H.-Y.; Jeong, D. H.; Kim, J.-H., Single-Step and Rapid Growth of Silver Nanoshells as SERS-Active Nanostructures for Label-Free Detection of Pesticides. *ACS applied materials & interfaces* **2014,** *6* (15), 12541-12549.

28. Stöber, W.; Fink, A.; Bohn, E., Controlled growth of monodisperse silica spheres in the micron size range. *Journal of colloid and interface science* **1968,** *26* (1), 62-69.

29. (a) Biswas, A.; Eilers, H.; Hidden, F.; Aktas, O.; Kiran, C., Large broadband visible to infrared plasmonic absorption from Ag nanoparticles with a fractal structure embedded in a Teflon AF® matrix. *Applied physics letters* **2006,** *88* (1), 013103-013103-3; (b) Genov, D. A.; Sarychev, A. K.; Shalaev, V. M., Metal-dielectric composite filters with controlled spectral windows of transparency. *Journal of Nonlinear Optical Physics & Materials* **2003,** *12* (04), 419-440.

30. (a) Ono, M.; Hirata, A.; Kometani, T.; Miyagawa, M.; Ueda, S.-i.; Kinoshita, H.; Fujii, T.; Kuwano, M., Sensitivity to gefitinib (Iressa, ZD1839) in non-small cell lung cancer cell lines correlates with dependence on the epidermal growth factor (EGF) receptor/extracellular signal-regulated kinase 1/2 and EGF receptor/Akt pathway for proliferation. *Molecular cancer therapeutics* **2004,** *3* (4), 465-472; (b) Menju, T.; Hashimoto, S.; Hashimoto, A.; Otsuka, Y.; Handa, H.; Ogawa, E.; Toda, Y.; Wada, H.; Date, H.; Sabe, H., Engagement of overexpressed Her2 with GEP100 induces autonomous invasive activities and provides a biomarker for metastases of lung adenocarcinoma. *PloS one* **2011,** *6* (9), e25301.

Abstract in Korean

표면증강 라만산란 (SERS) 이란 금이나 은 같은 귀금속 표면에 분자가 흡착되었을 때, 분자의 라만 산란 신호가 크게 증가하는 현상으로, 생체 내 진단이나 이미징과 같은 분석 분야에 적용될 수 있는 매우 민감한 진동 분광 기술을 말한다. 이 기술은 비활성 귀금속 나노 입자와 특정 라만 표지 분자가 합쳐진 SERS tag이라 불리는 물질을 이용하여 활용되고 있다. 그러나, 기존의 일반적인 SERS tag의 합성 방법은 여러 단계로 이루어지거나, 낮은 신호 안정성을 보인다는 한계점을 보인다. 이전에 실리카 나노 입자를 기반으로 한 은 나노쉘의 단일 단계 합성 방법이 보고된 바 있다. 본 연구에서는 이 은 나노쉘 합성법에서 더 발전시켜, 매우 증강된 라만 신호를 유도할 수 있는 나노갭 구조를 가진 SERS tag을 단일 단계로 합성하는 방법에 대해 연구하였다. 은 나노갭 범피쉘은 성공적으로 단일 단계로 합성되었고, SERS 세기 증가에 용이한 거친 표면을 가지고 있으면서, 동시에 은 표면에 나노갭을 가진 구조를 보였다. 이 특이한 은 나노갭 범피쉘은 반응물에 작은 라만 표지 분자를 처음부터 넣어줌으로써, 은 나노 입자가 형성될 때 실리카 표면에 은 나노 입자와 라만 표지 분자가 동시에 흡착되면서 만들어지게 된다. 또한, 은 나노갭 범피쉘은 기존의 합성 방법으로 만들어진 은 나노쉘 기반의 SERS tag에 비해 3.5 배 이상 증강된 라만 신호 세기와 좋은 신호 안정성을 보였다. 라만 표지 분자를 달리하여 다양한 은 나노갭 범피쉘을 합성하였으며, 생체 내 다수의 표적물에 대한 다중 측정

이미징을 위한 SERS tag으로 사용할 수 있는 가능성을 보여주었다.

주요어: 표면 증강 라만 산란, 나노쉘, 나노갭, 다중 측정

학번: 2013-20987